Acta Oceanol. Sin., 2015, Vol. 34, No. 5, P. 103–109
DOI: 10.1007/s13131-015-0673-0
http://www.hyxb.org.cn
E-mail: hyxbe@263.net

A mathematical model of calculating local tsunami wave source constraints and propagation

LI Daming[1]*, LI Yangyang[1]

[1] State Key Laboratory of Hydraulic Engineering Simulation and Safety, Tianjin University, Tianjin 300072, China

Received 23 May 2014; accepted 21 October 2014

Abstract

This paper presents a local tsunami simulation, including the initial displacement field model of tsunami source and tsunami wave propagation model. We deduced the tsunami wave equation; applied the matching of interior and exterior solutions method and water mass method to determine the initial displacement field in different bottom topography. Tsunami wave propagation model was based on the Boussinesq equation. Difference format was based on the ADI method which discretized in alternating direction in the form of implicit scheme. The open boundary of ADI had been revised considering the influence of wave propagation in the equation of motion. The local tsunami mathematical model was used in the simulation of 2011 Japan tsunami, and the results and the observation data match well.

Key words: local tsunami, initial displacement field, numerical simulation, tsunami wave propagation

Citation: Li Daming, Li Yangyang. 2015. A mathematical model of calculating local tsunami wave source constraints and propagation. Acta Oceanologica Sinica, 34(5): 103–109, doi: 10.1007/s13131-015-0673-0

1 Introduction

Tsunami is a kind of destructive and disastrous wave. In recent years, tsunami assaulted globally. On December 26, 2004 in northwest Sumatra, tsunami happened in the Indian Ocean causing more than 300 thousand fatalities. On July 17, 2006, the Indian Ocean tsunami in Indonesia has left at least 668 people dead, 1 438 wounded, and 287 missing. On February 27, 2010, tsunami hit Chile and 214 people died in the disaster. On March 11, 2011 tsunami struck Japan Hokkaido, Aomori, Iwate, Miyako, Fukushima and Ibaraki Prefecture, more than 10 000 people died. The following nuclear radiation from Fukushima has impacted severely Japan and peripheral areas.

Until recently, there is some lack of knowledge about making a scientific prediction of changes in the earth's crust 1–2 days in advance as undersea earthquake happened and resulted tsunami, the main protection method is through artificial warning system such as alarm, telephone, the weather forecast radio, an emergency alert system, etc. (Darienzo, 2005; Geist et al., 2007; Igarashi et al., 2011; McCreery, 2005; Frolov et al., 2012). The tsunami early warning work involves action time and forecast accuracy, et al. Initial displacement field model and wave propagation model of tsunami have been discussed by many researchers. Grilli et al. (2009) used a probabilistic approach for determining submarine landslide tsunami hazard along the upper east coast of the United States which results were presented in terms of nearshore breaking wave height and runup, caused by seismically induced tsunami genic SMF, with a given return period. For 2011 Japan tsunami, Grilli et al. (2013) simulated the 2011 M9 Tohoku–Oki tsunami using new coseismic tsunami sources based on inverting onshore and offshore geodetic data, using 3D Finite Element Models (FEM), which FEMs simulated elastic dislocations along the plate boundary interface separating the stiff subducting Pacific Plate from the relatively weak forearc and volcanic arc of the overriding Eurasian plate. Wang et al. (2012) simulated the Japan Mw9.0 earthquake on March 11 in 2011 and analyzed tsunami propagating and its impact on Chinese coasts. Yan et al. (2014) simulated the wave propagation using Centroid Moment Tensor (CMT) which as the epicenter source and PREM earth model. Ren et al. (2013) used Okada's elastic fault model to generate the deformation of the sea bottom based on USGS sources and UCSB sources respectively. The shallow water equations were solved by the adaptively refined finite volume methods so that it can compute the propagation of tsunami in the Pacific Ocean efficiently. Yuan et al. (2013) proposed a comprehensive method using wavelet energy spectrum analysis, power spectrum analysis and filtering analysis to extract tsunami wave and used COMCOT model for tsunami wave. Jing et al. (2013) used the tsunami modeling results to verify earthquake constraints on finite fault models.

Considerable work has been completed on the tsunami numerical simulation studies focused on the damage modeling, Geophysical observations, tsunami deposits, flow speed, wave hazards and vulnerability, etc. (Tychsen et al., 2008; Simons et al., 2011; Szczuciński, 2012; Jaffe and Gelfenbuam, 2007; Cochard et al., 2008). The present mathematical model based on theoretical equation can be divided into four categories (Li et al., 2009): the first kind is based on the long wave equation shallow water theory model, this kind of model is the most widely used by Japanese Tohoku university as TUNAMI2N2 model which has passed TIME (Tsunami Inundation Modeling Exchange) plan and is widely used all over the world in the Tsunami research; in addition, NOAA tsunami research center (NCTR)'s MOST introduc-

Foundation item: The National Natural Science Foundation of China under contract No. 51079095; the Science Fund for Creative Research Groups of the National Natural Science Foundation of China under contract No. 51021004.
*Corresponding author, E-mail: lidaming@tju.edu.cn

tion model, COMCOT model of Cornell University as well as our country business change model (CBCM), etc., belong to this category. The COMCOT model has been applied in southwestern Taiwan tsunami warning system and the influential analysis of tsunami to Sri Lanka in 2004 (Wijetunge, 2009), etc. The second kind is based on the model based on Boussinesq equation such as classical Boussinesq and the Boussinesq improved by Delaware University. The third type is based on the fully nonlinear potential flow theory model. The fourth type is based on the Navier–Stokes equation model.

Most initial displacement field based on the fault model which assuming crust broken deformation is the initial displacement field. This paper established a local tsunami model based on tsunami wave theory equation by matching the interior and exterior solutions method to determine the initial displacement field of tsunami wave. This initial displacement field method supplies the progress from the crest broken to initial wave. The ADI method had been used in the propagation model and was improved in terms of boundary and energy transfer. Finally, this model is applied in the simulation of Japanese tsunami in 2011.

2 The establishment of tsunami numerical model

The establishment of tsunami numerical model consists of two parts. One is the tsunami source constraints model of the initial displacement field of tsunami; the other part is the tsunami wave propagation model which is calculated based on the Boussinesq equation.

2.1 *The initial displacement field of tsunami*

There is some hypothesis: sea water is ideal incompressible liquid, the movement of the sea water is potential that irrotational motion and the seawater movement wave height are small. Thus, the problem boils down to find the velocity potential. On the one hand, the potential function should satisfy the Laplace equation. It should satisfy the boundary and initial conditions on the other hand.

(1) The Laplace equation

$$\frac{\partial^2\phi}{\partial x^2}+\frac{\partial^2\phi}{\partial y^2}+\frac{\partial^2\phi}{\partial z^2}=0. \tag{1}$$

(2) Boundary conditions

When $z=0$, to meet the dynamics conditions:

$$\frac{\partial\phi}{\partial t}=g\eta, \tag{2}$$

when $z=-h$, if there exists the external force on the water surface (including the sudden lifting of the sea level):

$$\frac{\partial\phi}{\partial z}=0. \tag{3}$$

If considering the earthquake result in sea floor uplifted, the change in speed of the seabed satisfies the equation:

$$\frac{\partial\phi}{\partial z}=f(x,y)h(t). \tag{4}$$

There can be made a variety of combinations between the range of seafloor $f(x,y)$ and the range of $h(t)$. And the initial condition also should be considered necessarily.

(3) The derivation of the theoretical solution of the tsunami wave equation

When the tsunami occurred, the situation of the sea floor variation was shown in Fig. 1.

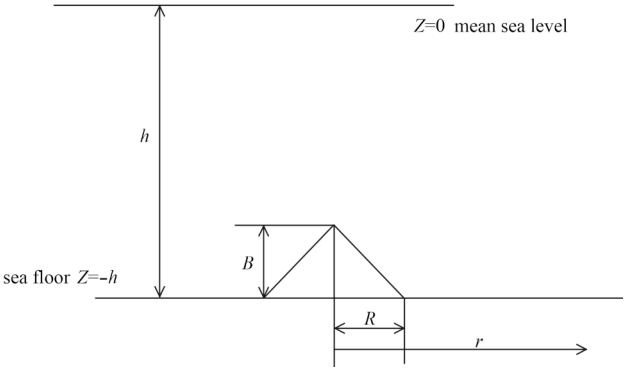

Fig. 1. Situation of the sea floor variation.

The shape of uplifted area in the bottom of the sea is conical, where R is the radius; B is the maximum height of the uplifted area. In the conical region, when $r>R$, the Laplace Eq. (1) could transform by the Cartesian coordinate system to the cylindrical coordinate system as follows:

$$\frac{1}{\rho}\frac{\partial}{\partial\rho}\left(\rho\frac{\partial\phi}{\partial\rho}\right)+\frac{1}{\rho^2}\frac{\partial^2\phi}{\partial\lambda^2}+\frac{\partial^2\phi}{\partial z^2}=0. \tag{5}$$

The method of separation of variables was applied to separate the velocity potential function ϕ as the form that is the product of the space function $\varphi(\rho,\lambda,z)$ and time function $T(t)$, $\phi(\rho,\lambda,z,t)=\varphi(\rho,\lambda,z)\,T(t)$. The method of separation of variables was applied to space function again and φ was isolated form $\varphi(\rho,\lambda,z)=K(\rho)\,Q(\lambda)\,Z(z)$ then get equation:

$$\frac{1}{K}\frac{1}{\rho}\frac{\partial}{\partial\rho}\left(\rho\frac{\partial K}{\partial\rho}\right)=-\frac{1}{Z}\frac{\partial^2 Z}{\partial z^2}. \tag{6}$$

Through the above method, the solution can be summarized as follows.

When $r>R$ (outside the tsunami lifted area), the equation was solved by the Laplace equation adding the homogeneous boundary conditions into the equation, then we get the tsunami volatility expressions:

$$\eta=\frac{\sigma E}{g}\cosh k(h+z)\,J_0(kr)\cos(\sigma t+\varepsilon), \tag{7}$$

where $k=-\mu$, σ can be got from $\sigma^2=gk\tanh k(h+z)$, $J_0(k\rho)$ is a rectifiable zero order of the first class Bessel function, ε is a slight phase difference variable, E is a constant.

When $r\leqslant R$ (inside the tsunami lifted area), also satisfies the Laplace equation and then put the non-homogeneous boundary conditions into the equation, get the expression of tsunami volatility

$$\eta'=\frac{mFJ_0(kr)\,\mathrm{e}^{-mt}}{gk(gk\sinh kh+m^2\cosh kh)}\left(gk\cosh kz-m^2\sinh kz\right). \tag{8}$$

(4) The establishment of the initial displacement field

Because of Bessel functions with the volatility, in the seabed deformation zone, the fluctuation of the sea floor should be consistent with the fluctuation of the sea level. To get the smallest root of Bessel function we establish the equation $J_0(x_0)=0$ through making coordinate transformation of r, then $r=x_0r'/kR$ can be obtained. By the use of interior and exterior solutions matching method (Qian, 1981) (the wave amplitude of tsunami match for $r\leqslant R$ and $r\geqslant R$) a tsunami wave function at sea surface was ob-

tained. The interior solution of waters is (Xue et al., 1980)

$$\eta = C\,\frac{\sigma F J_0(kr)\mathrm{e}^{-\sigma t}}{gk[\sinh(kD)+\sigma^2\cosh(kD)]}\,, \tag{9}$$

where $F=\dfrac{1}{\sqrt{2}}B\sigma R J_1(kR)$, σ is the wave frequency,

$$\sigma=\begin{cases}\sqrt{gk} & D/L>1/2 \quad \text{deepwater}\\ \sqrt{gk\tanh(kD)} & 1/2>D/L>1/20\\ k\sqrt{gD} & D/L<1/20 \quad \text{shallowwater}\end{cases},$$

where k is wave number; B is the deformation height of the seafloor; R is the radius of deformation seafloor; t is the time of sea floor deformation; r is the distance from the displacement point to source; $J_0(kr)$ is Zeroth-order Bessel function; $J_1(kR)$ is first-order Bessel function; C is deformation volume factor of the seabed and the sea level.

For circular uplift and collapse seabed deformation, initial water surface displacement field was shown in Fig. 2.

For long and narrow seafloor, the initial water surface displacement field including uplift and collapse, take the following two cases into consideration as shown in Fig. 3.

Despite the difference between changes in morphology of the sea level and seabed, but the changes in both volumes are equal which thereby determine the circular deformation volume factor C=1.464 and the narrow shape deformation volume factor C=1.548.

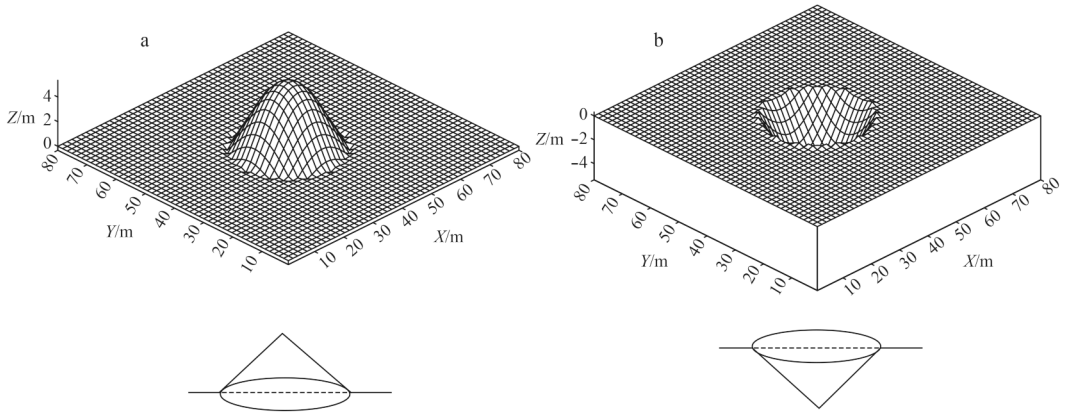

Fig. 2. Water surface initial displacement field caused by the circular seabed deformation: a. circular uplift seabed deformation and b. circular collapse seabed deformation.

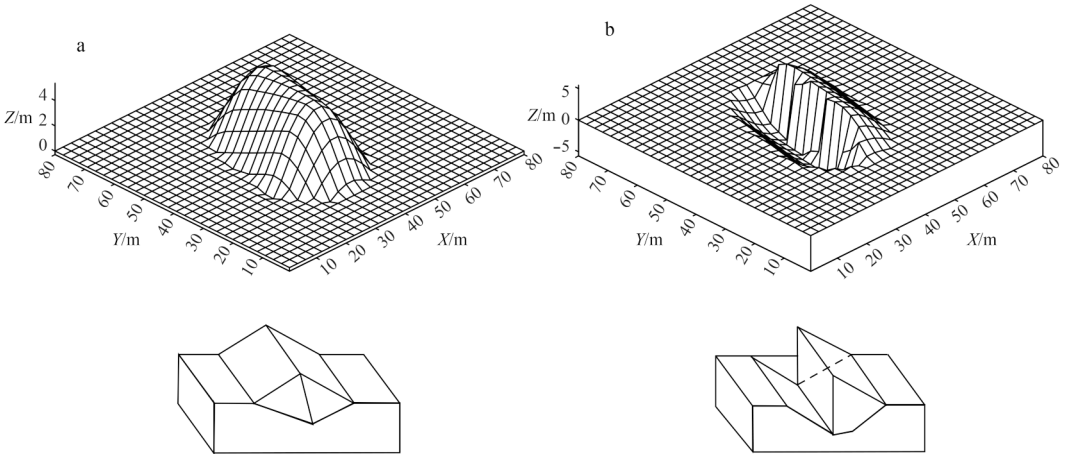

Fig. 3. Water surface initial displacement caused by the deformation of long and narrow: a. narrow uplift seabed deformation and b. narrow uplift seabed dislocation deformation.

2.2 *The two dimensional governing equation in the local tsunami*

The local tsunami is a kind of offshore tsunami which the tsunami hypocenter and the affected areas are in the same area. Water depth is shallow in offshore areas, non-convective term increases, the Coriolis force is so small which can be neglected, the bottom friction increases, so the governing equation uses the two-dimensional Boussinesq equation which considers bottom friction. The expression of the equation in Cartesian coordinate's form is

$$\frac{\partial\eta}{\partial t}+\frac{\partial}{\partial x}\left[(\eta+h)u\right]+\frac{\partial}{\partial y}\left[(\eta+h)v\right]=0, \tag{10}$$

$$\frac{\partial u}{\partial t}+u\frac{\partial u}{\partial x}+v\frac{\partial u}{\partial y}+g\frac{\partial\eta}{\partial x}+\frac{gu\sqrt{u^2+v^2}}{C^2(\eta+h)}=\frac{\eta+h}{2}\left[\frac{\partial^3 u(\eta+h)}{\partial x^2\partial t}+\frac{\partial^3 v(\eta+h)}{\partial x\partial y\partial t}\right]-\frac{(\eta+h)^2}{6}\left(\frac{\partial^3 u}{\partial x^2\partial t}+\frac{\partial^3 v}{\partial x\partial y\partial t}\right), \tag{11}$$

$$\frac{\partial v}{\partial t}+u\frac{\partial v}{\partial x}+v\frac{\partial v}{\partial y}+g\frac{\partial \eta}{\partial y}+\frac{gv\sqrt{u^2+v^2}}{C^2(\eta+h)}=\frac{\eta+h}{2}\left[\frac{\partial^3 v(\eta+h)}{\partial y^2\partial t}+\frac{\partial^3 u(\eta+h)}{\partial x\partial y\partial t}\right]-\frac{(\eta+h)^2}{6}\left(\frac{\partial^3 v}{\partial y^2\partial t}+\frac{\partial^3 u}{\partial x\partial y\partial t}\right), \tag{12}$$

where η is the displacement of the free surface relative to the mean sea level; u and v are the x and y components of the water velocity vector. h is the water depth, C is the Chézy coefficient, $C=\frac{1}{n}(\eta+h)^{\frac{1}{6}}$, n is the roughness coefficient.

2.3 *The discretization of governing equation considering the transfer of tsunami wave field energy*

Tsunami wave propagation power depends on the water surface slope and the water energy transmission. The transfer of the speed is considered in the traditional ADI difference scheme only. The impact of the energy transfer was considered on the basis of the original ADI method in this paper. And we applied widely used finite volume ideological integration into the ADI method considered the epicenter fluctuations vibration intensive. Equations (11) and (12) add the term of energy changes as the form of radiation stress that is

$$\begin{cases} T_x=-\dfrac{1}{\rho h}\dfrac{\partial E}{\partial x} \\ T_y=-\dfrac{1}{\rho h}\dfrac{\partial E}{\partial y} \end{cases}.$$

The energy term is based on wave energy equilibrium equation of Маккавеев

$$\frac{\partial E}{\partial t}+\frac{\partial U_E E}{\partial x}=W_f-W_\mu, \tag{13}$$

where E is the wave energy per unit area in the water column; $E=\frac{1}{8}\rho g H^2$, W_f is the energy that wind passed to wave, for tsunami wave, it means 0; $W_\mu=\frac{1}{18}\pi^3\rho g K^2\frac{H^4}{L^2T}$ is the loss rate of Wave internal friction energy ; K is coefficient, generally take 1.0. The integral for energy in the area of grids is

$$A\frac{\partial E}{\partial t}+\oint_l (E\bar{V}\cdot\bar{n})\mathrm{d}l=-AW_\mu. \tag{14}$$

The integral for energy in the area of grids is

$$E_i^{k+1}=E_i^k+\frac{\Delta t}{A}\sum_{n=1}^{N}Q_{\mathrm{in}}L_{\mathrm{in}}-\Delta tW_\mu, \tag{15}$$

where Q_{in} is the energy flux in the edge of the grid; L_{in} is the length of Grid side; A is the area of the grid.

2.4 *The processing of the water boundary conditions of local model*

In the ADI method, the water boundary conditions were given by external procedure, but because the change of boundary conditions caused by domain fluctuations. So the external procedure should be modified, the open boundary on the left is

$$S_{IS-1,j}=B^{(k)}_{IS-\frac{1}{2}j}+\frac{1}{2}\frac{\Delta t}{\Delta s}g\xi^{(k-\frac{1}{2})}_{IS-\frac{1}{2}j}. \tag{16}$$

The open boundary on the right is

$$u^{(k+\frac{1}{2})}_{IE+\frac{1}{2}j}=\frac{B^{(k)}_{IS-\frac{1}{2}j}+\frac{1}{2}\frac{\Delta t}{\Delta s}g(Q_{IE,j}-\xi^{(k-\frac{1}{2})}_{IE-\frac{1}{2}j})}{1+\frac{1}{2}\frac{\Delta t}{\Delta s}gP_{IE,j}}. \tag{17}$$

3 Example simulation

This mathematical model was applied to simulate the tsunami which happened in Japan on March 11, 2011. The distance is 130 km between epicenter and the nearest costal city Sendai (38.1°N, 142.6°E), and the focal depth is about 20 km. Table 1 lists the main hypocenter parameters obtained from United States Geological Survey (USGS).

Table 1. The parameters of hypocenter obtained from United States Geological Survey

Fault length L/km	Fault width W/km	Mean slip D/m	Dip σ/(°)	Slip angle λ/(°)	Fault strik θ/(°)	The distance between submarine and the top surface of fault H/km
400	150	20	14	81	14	10

The initial displacement of water surface according to the calculation of the theoretical solution (referred in Section 1.1) and topographical condition were from the USGS, the initial displacement field is shown in Fig. 4.

In the calculation of tsunami wave transmission, model range of computational domain was 34°–43°N, 140°–50°E. The time step was 4 s. Rectangular grids were applied which size was. Simulating a wave field in one hour after the tsunami happened, Fig. 5 showed the change of tsunami wave field at 15, 30, 45, 60 min.

According to the time process curves of tsunami wave, we have chosen 7 points in the model to represent the locations of hypocenter, Choshi, Sendai, Kesennum, Ishinomaki, Miyako and DART buoy 21418 specific locations referred in Fig. 4b. Figure 6 shows the model results in the above locations. Table 2 shows the comparison between simulated wave height and maximum wave height observed on the bank. Records from news reports (http://www.youtube.com/watch?v=X6GzxcXsecg) show that tsunami waves attacked Choshi, after earthquake occurred 20 min, then it attacked Sendai 15 min later. At last, the tsunami waves arrived at Miyako. Residents at the scene (field personnel) hold that wave height arrived almost 10 m. In approximately 25 min, the tsunami was first recorded at DART® buoy 21418. The DART system is managed and operated by National Oceanic and Atmospheric Administration (NOAA). The No. 21418 buoy is located in the northeast of Tokyo (38°42'38"N, 148°41'37"E), and depth there is 5 685 m, the sequence of attacking basically correspond to the people at the scene observed as shown in Table 2. The simulation time of Miyako is earlier than its observed time. The calculating results of No. 21418 buoy agree well with the observed ones in the maximum wave height and appearance time. Figure 7 shows the comparison between model results and observed data of No. 21418 buoy. The maximum tsunami wave height is almost 2 m among the data monitored by No. 21418 buoy.

The maximum height of wave observed at DART 21418 was almost 2 m, which are in good agreement with model results in time. As shown in Table 2 the model order meets well while sim-

ulated tsunami arriving Miyako earlier.

4 Conclusions

In the process of building the initial field, we deduced tsunami wave theory equation and used the method of matching inner and out solutions to set up condition initial field. Considering initial field had different forms, different shape deformations had equal water volume, we established the concept of volume coefficient and calculated two forms' volume coefficient. The results show the hydrodynamic method calculating the initial displacement is feasible. In the tsunami wave propagation model, we discretized the Boussinesq equation which considering the bottom friction. On the basis of ADI difference format we supplemented Energy spread item and further deal with the boundary conditions.

Using this local tsunami model with model grid 4 km by 4 km regular mesh we simulated tsunami in Japan in March, 2011. Comparing with 7 feature points in including five stations: Choshi, Miyako, Kesennum, Ishinomaki and Sendai, Dart buoy 21418 and hypocenter, we found reasonable agreement between model simulations and observed tsunami wave height. In the comparison of the model and observed tsunami arrival time at

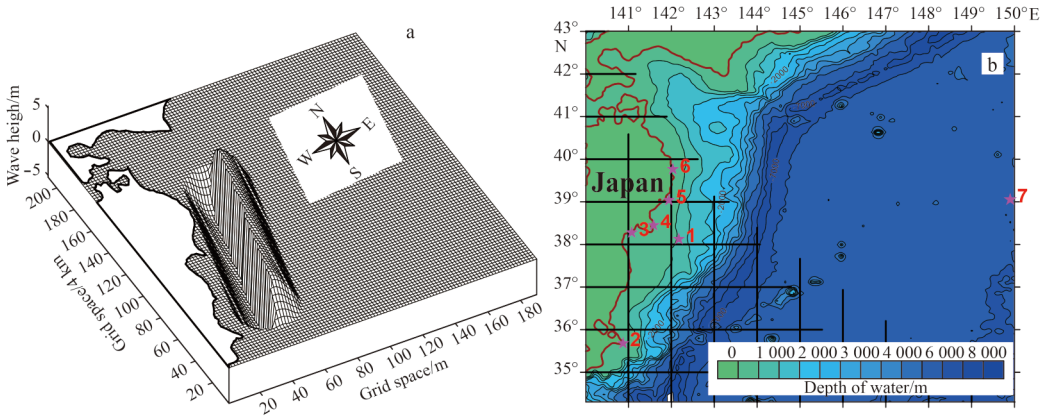

Fig. 4. The initial displacement of water surface according to the calculation of the theoretical solution (a) and the topographical condition around the epicenter and the model range (b).

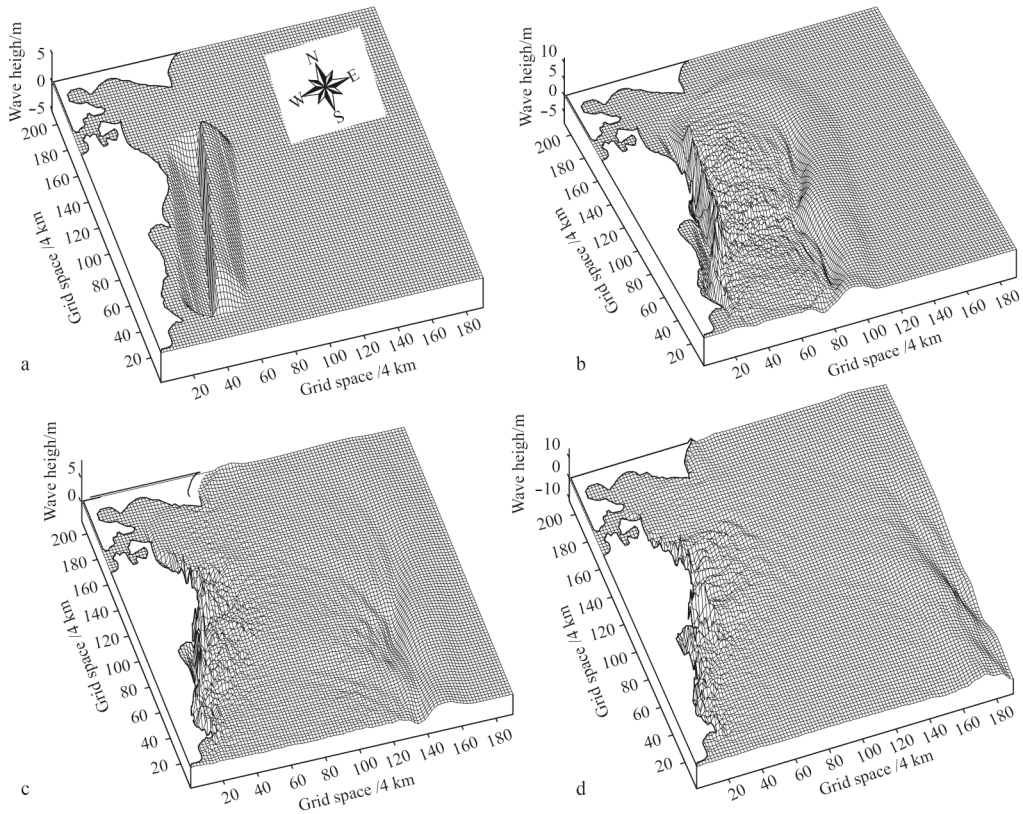

Fig. 5. The wave field after the tsunami happened 15 min (a), the wave field after the tsunami happened 30 min (b), the wave field after the tsunami happened 45 min (c) and the wave field after the tsunami happened 60 min (d).

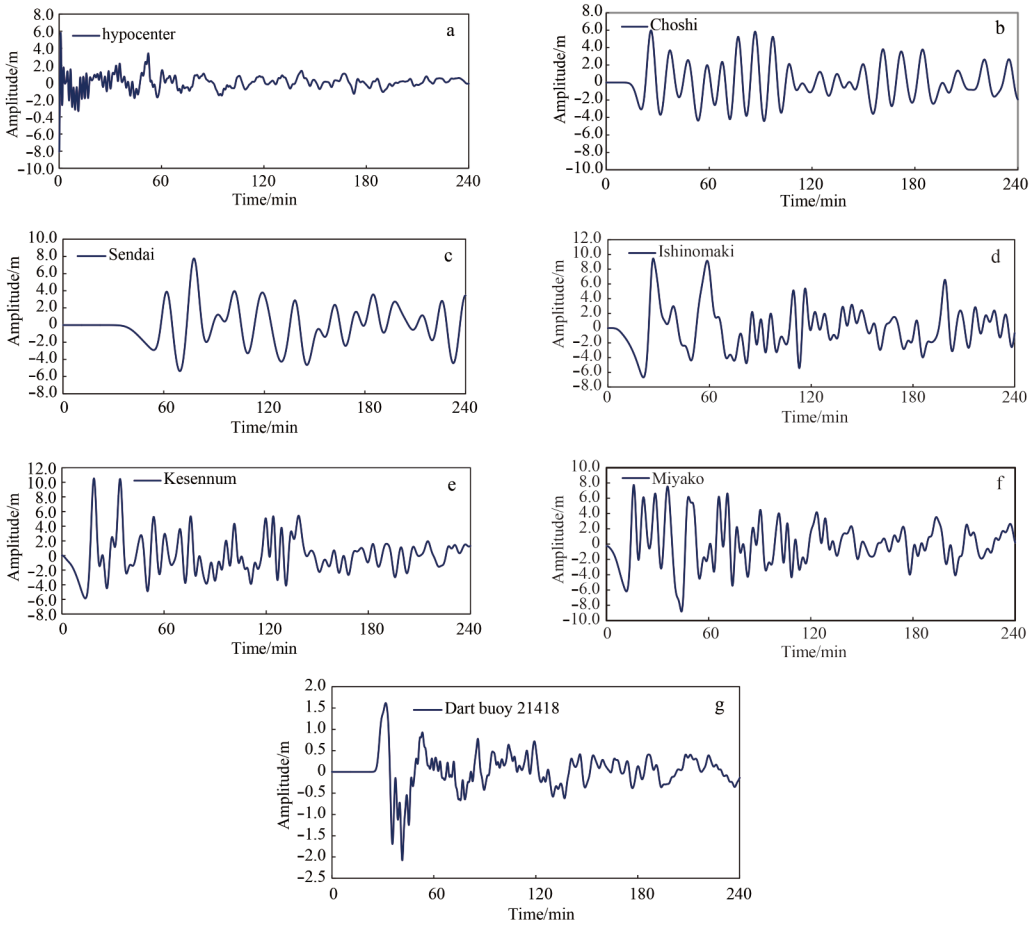

Fig. 6. The simulation results for 7 feature points (specific location referred in Fig. 4b). a. The wave height of tsunami: hypocenter, b. the wave height of tsunami: Choshi, c. the wave height of tsunami: Miyako, d. the wave height of tsunami: Kesennum, e. the wave height of tsunami: Ishinomaki, f. the wave height of tsunami: Sendai, and g. the wave height of tsunami: No. 21418 buoy.

Table 2. The comparison between simulated wave height and maximum wave height observed on the bank

Location	Maximum wave height observed on the bank/km	Simulated max. wave height/m	Simulated wave-generation time/min	Simulated appearance time of max. peak/min	Observed tsunami arrival time/min
Hypocenter	–	8.06	1	1	–
Choshi	6	5.97	7	26	–
Miyako	10	7.73	1	16	35+
Kesennum	–	10.52	1	19	20
Ishinomaki	10	9.45	9	27	–
Sendai	10	7.76	22	78	35
DART 21418 buoy	2	1.62	22	32	25

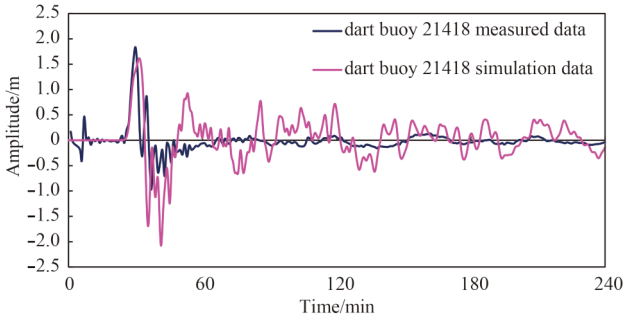

Fig. 7. Comparison between observed data of DART system (dark bule) and model results of No. 21418 buoy (pinkish red).

different stations, tsunami arrived Miyako earlier mainly due to the tsunami wave propagation time to each station determined by fault strike and initial field parameters and intensity. We expect to refine the model through obtaining more accurate and detailed data, and an improved way of adjusting hypocenter parameter is suggested for further study. After 60 min model has an obvious tsunami reflection phenomenon related the limited local tsunami wave simulation boundary, we are working on a slip boundary to resolve this problem and have a certain effect. This simulation model is quite fine for the highest wave height of Dart buoy 21418; besides the model wave height is higher after 60 min which may result from the loss coefficient and energy attenuation. But because the key issue of tsunami warning is arrival time and the maximum wave height, this model is applicable.

References

Cochard R, Ranamukhaarachchi S L, Shivakoti G P, et al. 2008. The 2004 tsunami in Aceh and Southern Thailand: A review on coastal ecosystems, wave hazards and vulnerability. Perspectives in Plant Ecology, Evolution and Systematics, 10(1): 3–40

Darienzo M, Aya A, Crawford G L, et al. 2005. Local Tsunami warning in the Pacific coastal United States. Natural Hazards, 35(1): 111–119

Frolov A V, Kamaev D A, Martyshchenko V A, et al. 2012. Experience of the Russian tsunami warning system updating. Russian Meteorology and Hydrology, 37(6): 357–368

Geist E L, Titov V V, Arcas D, et al. 2007. Implications of the 26 December 2004 Sumatra–Andaman earthquake on tsunami forecast and assessment models for great subduction–zone earthquakes. Bulletin of the Seismological Society of America, 97(1A): S249–S270

Grilli S T, Harris J C, Tajalli Bakhsh T S, et al. 2013. Numerical simulation of the 2011 Tohoku Tsunami based on a new transient FEM co–seismic source: comparison to far-and near-field observations. Pure and Applied Geophysics, 170(6–8): 1333–1359

Grilli S T, Taylor O D S, Baxter C D P, et al. 2009. A probabilistic approach for determining submarine landslide tsunami hazard along the upper east coast of the United States. Marine Geology, 264(1–2): 74–97

Igarashi Y, Kong L, Yamamoto M, et al. 2011. Anatomy of Historical Tsunamis: lessons learned for tsunami warning. Pure and Applied Geophysics, 168(11): 2043–2063

Jaffe B E, Gelfenbuam G. 2007. A simple model for calculating tsunami flow speed from tsunami deposits. Sedimentary Geology, 200(3–4): 347–361

Jing Huimin, Zhang Huai, Wu Zhongliang, et al. 2013. Tsunami constraints on finite fault models: the March 11, 2011 Tohoku earthquake. Earthquake (in Chinese), 33(4): 207–213

Li Daming, Fu Qingjun, Lin Yi. 2009. Research on the local tsunami wave propagation mathematical model. Ocean Technology (in Chinese), 28(1): 60–65

McCreery C S. 2005. Impact of the national tsunami hazard mitigation program on operations of the richard H. Hagemeyer Pacific Tsunami warning center. Natural Hazards, 35(1): 73–88

Qian Weichang. 1981. Singular Perturbation Theory and Its Applications in Mechanics (in Chinese). Beijing: Science Press, 87–131

Ren Zhiyuan, Wang Benlong, Fan Tingting, et al. 2013. Numerical analysis of impacts of 2011 Japan Tohoku tsunami on China Coast. Journal of Hydrodynamics, Ser B, 25(4): 580–590

Simons M, Minson S E, Sladen A, et al. 2011. The 2011 magnitude 9. 0 Tohoku–Oki earthquake: mosaicking the megathrust from seconds to centuries. Science, 332(6036): 1421–1425

Szczuciński W. 2012. The post-depositional changes of the onshore 2004 tsunami deposits on the Andaman Sea coast of Thailand. Natural Hazards, 60(1): 115–133

Tychsen J, Geertz-Hansen O, Schjøth S. 2008. KenSea-tsunami damage modelling for coastal areas of Kenya. Geological Survey of Denmark and Greenland Bulletin, 15: 85–88

Wang Peitao, Yu Fujiang, Zhao Lianda, et al. 2012. Numerical analysis of tsunami propagating generated by the Japan Mw9. 0 earthquake on Mar. 11 in 2011 and its impact on China coasts. Chinese Journal of Geophysics (in Chinese), 55(9): 3088–3096

Wijetunge J J. 2009. Field measurements and numerical simulations of the 2004 tsunami impact on the south coast of Sri Lanka. Ocean Engineering, 36(12–13): 960–973

Xue Hongchao, Gu Jialong, Ren Rushu. 1980. Coastal Dynamics. Beijing: China Communications Press (in Chinese), 286–306

Yan Zhenzhen, Zhang Huai, Fan Xiangtao, et al. 2014. Comparative analysis of the characteristics of global seismic wave propagation excited by the Mw 9. 0 Tohoku earthquake using numerical simulation. Science China Earth Sciences, 57(7): 1626–1636

Yuan Chuguang, Wang Yigang, Huang Huiming, et al. 2013. Impact of "311" Japan tsunami on northern Jiangsu coast. The Ocean Engineering (in Chinese), 31(6): 68–75